

Article

Optical Properties of AgInS₂ Quantum Dots Synthesized in a 3D-Printed Microfluidic Chip

Konstantin Baranov^{1,*}, Ivan Reznik^{1,2,*}, Sofia Karamysheva¹, Jacobus W. Swart², Stanislav Moshkalev³ and Anna Orlova^{1,*}

- ¹ International Laboratory Hybrid Nanostructures for Biomedicine, ITMO University, Saint Petersburg 199034, Russia; spkaramysheva@itmo.ru
² Faculty of Electrical Engineering and Computing, University of Campinas, Campinas 13083-970, Brazil; jacobus@unicamp.br
³ Centre for Semiconductor Components and Nanotechnology, University of Campinas, Campinas 13083-870, Brazil; stanisla@unicamp.br
* Correspondence: baranov.const@mail.ru (K.B.); ivanreznik1993@mail.ru (I.R.); a.o.orlova@gmail.com (A.O.)

Abstract: Colloidal nanoparticles, and quantum dots in particular, are a new class of materials that can significantly improve the functionality of photonics, electronics, sensor devices, etc. The main challenge addressed in the article is modification of the syntheses of colloidal NP to launch them into mass production. It is proposed to use an additive printing method of chips for microfluidic synthesis, and it is shown that our approach allows to offer a cheap, easily scalable and automated synthesis method which allows to increase the product yield up to 60% with improved optical properties of AgInS₂ quantum dots.

Keywords: microfluidic synthesis; 3D printing; colloidal luminescent quantum dots; optical properties



Citation: Baranov, K.; Reznik, I.; Karamysheva, S.; Swart, J.W.; Moshkalev, S.; Orlova, A. Optical Properties of AgInS₂ Quantum Dots Synthesized in a 3D-Printed Microfluidic Chip. *Technologies* **2023**, *11*, 93. <https://doi.org/10.3390/technologies11040093>

Academic Editors: Sergey N. Grigoriev and Nam-Trung Nguyen

Received: 19 May 2023
Revised: 25 June 2023
Accepted: 10 July 2023
Published: 12 July 2023



Copyright: © 2023 by the authors. Licensee MDPI, Basel, Switzerland. This article is an open access article distributed under the terms and conditions of the Creative Commons Attribution (CC BY) license (<https://creativecommons.org/licenses/by/4.0/>).

1. Introduction

Quantum dots (QD) are a striking representative of a new class of luminophores and colloidal nanoparticles simultaneously. The challenge today is to develop new synthesis methods that are easily scalable and automated. The temperature and mixing rate of precursors during the formation of structures have a huge impact on their optical properties such as the position, shape and width of the photoluminescent (PL) band and the PL quantum yield (PLQY) of quantum dots [1,2]. It is well known that reproducing the synthesis of nanoparticles using the same technique with classical hydrothermal synthesis might cause unstable results due to human factors, limiting the nanostructures production on an industrial scale and their application in medicine [3]. Microfluidic synthesis is the introduction of reagents through programmable syringe pumps, which allows a continuous supply of precursors at a certain rate and automation of the system to produce the required particles [4]. In addition, a large number of microfluidic chip channels can ensure efficient mixing of reagents. These advantages of microfluidic methods over traditional ones have motivated the development, fabrication, and use of inexpensive devices that allow precise temperature control and efficient reagent mixing [5]. All the characteristics mentioned above make microfluidics very advantageous for various applications, from chemical, biological, and material industries to pharmacy and clinical diagnostics [6,7].

Most research groups are focused on using a soft lithography method in order to manufacture microfluidic devices [8]. However, this technology is time-consuming and expensive. For example, in [9], the chip fabrication for QD synthesis took about 30 h. Three-dimensional printing for the formation of microfluidic chips is an emerging trend, and the growing number of publications on microfluidic synthesis confirms its relevance [10]. To the best of our knowledge, this is the first time when quantum dots were synthesized in

exclusively 3D-printed microfluidic chips. Here, we suggest a new approach to manufacturing microfluidic chips for QD syntheses that can simplify the formation, reduce the cost of materials used, and significantly save time on commissioning the final product. The yield of the production of AgInS₂ (AIS) QD was 1.5 times higher than that of the classical hydrothermal method of synthesis in a flask.

Among different types of quantum dots, the most studied group is CdX (X = S, Se, Te), but the high cytotoxicity of cadmium hinders its wider application in biology and biomedicine and limits its mass use in photonic and electronic devices due to utilization problems [11]. Ternary quantum dots, including AIS QD, are the representatives of nanostructured luminophores with well-tuned optical properties, containing no heavy metal atoms [12]. Therefore, the development of approaches to their mass production will make it possible in the future to produce environmentally friendly nanostructured materials for use in photovoltaics, imaging, and sensorics [13]. In addition, it is well known that the AIS QD are capable of generating superoxide anion when exposed to UV- and visible range radiation due to their energy structure [14]. Interaction of such reactive oxygen species (ROS) with bacteria can lead to the destruction of the latter [15]. Therefore, the AIS QDs are potential candidates for the photodynamic therapy of bacteria [16]. Furthermore, such QD are characterized by a relatively simple hydrothermal synthesis procedure that could be easily transferred to continuous microfluidic synthesis [17].

In this work, it is shown that the use of additive printing to produce chips for microfluidic synthesis makes it possible to synthesize biocompatible colloidal AIS QDs whose luminescence properties are better than those of similar QDs synthesized at the same macroparameters (temperature, pressure and velocity of precursor pumping) by classical colloidal synthesis. Optical properties of AIS QDs synthesized by the microfluidic method and classical hydrothermal method in a flask were compared. It was demonstrated that the PLQY of the samples synthesized by the microfluidic method for 18 and 180 s was found to be 2.5 times higher than that of the samples synthesized in a flask. In addition, the increased yield of the product compared to the classical hydrothermal method, combined with full automation of the synthesis process, can significantly reduce the cost of the synthesized AgInS₂ quantum dots.

2. Materials and Methods

2.1. Chemicals

Indium (III) chloride (InCl₃), silver nitrate (AgNO₃), sodium sulfide (Na₂S × 9H₂O), ammonia hydrate (NH₄OH), mercaptoacetic acid (MAA), 2-propanol, and thioglycolic acid (TGA) were purchased from Sigma-Aldrich (St. Louis, MO, USA). All chemicals were used without further purification.

2.2. Quantum Dot AgInS₂ Synthesis

The reagents for the synthesis of the aqueous AIS QDs were mixed according to the procedure described in [17]. A mixture of precursors was formed and alternately added to 5 mL H₂O in the following order with respective concentrations: 0.052 mL AgNO₃ (0.1 M), 0.104 mL TGA (1M), 0.0334 mL NH₄OH (5M), 0.0364 mL InCl₃ (1M), 0.08 mL NH₄OH (5M), 0.052 mL (Na₂S × 9H₂O) (1M). Then, AIS QD syntheses were performed in a microfluidic chip and by the classical hydrothermal method in a flask, which is described in detail in Section 3.

2.3. Characterization Methods

The Anycubic Photon Mono 3D printer (Anycubic, Shenzhen, China) was used to fabricate the chip. The absorption spectra of the samples were recorded using a UV Probe 3600 spectrophotometer (Shimadzu, Kyoto, Japan). PL spectra were examined with a Cary Eclipse spectrofluorometer (Varian, Belrose, NSW, Australia). PL kinetics was analyzed using the Micro-Time100 single-photon counting microscope (PicoQuant, Berlin, Germany). Sample concentrations of AIS QDs were estimated using the methodology presented in [18].

The calculation of concentration for the studied samples is presented in Appendix A and Section 3.

The PLQY of the synthesized QDs was estimated relative to the PL quantum yield of rhodamine 6G according to Formula (1):

$$\varphi = \varphi_R \frac{I \cdot D_R \cdot n^2}{I_R \cdot D \cdot n^2}, \quad (1)$$

where n is the refractive index of the solvent, I is the integral luminescence intensity, and D is the optical density at the excitation wavelength of the sample. Index R refers to the parameters of the reference sample (rhodamine in ethanol). It should be noted that when calculating the integral luminescence intensity, the spectra cut at 800 nm were interpolated into the long-wavelength region, symmetrical to the short-wavelength region, in the Origin software package using the inversion operation.

The QDs luminescence decay times and amplitudes were estimated by approximating the experimental curves with Formula (2):

$$y = y_0 + \sum_{i=1}^n A_i \exp\left(\frac{-(x - x_0)}{\tau_i}\right), \quad (2)$$

where A_i is the amplitude of the i th component and τ_i is the characteristic decay time of the i th component.

3. Results and Discussion

3.1. Microfluidic Chip Formation

Photopolymer resin-based chips were prepared for nano- and microparticle microfluidic fusion. The microfluidic chip is shown in Figure 1 and is a continuous serpentine channel with a cross-section of 1 mm².

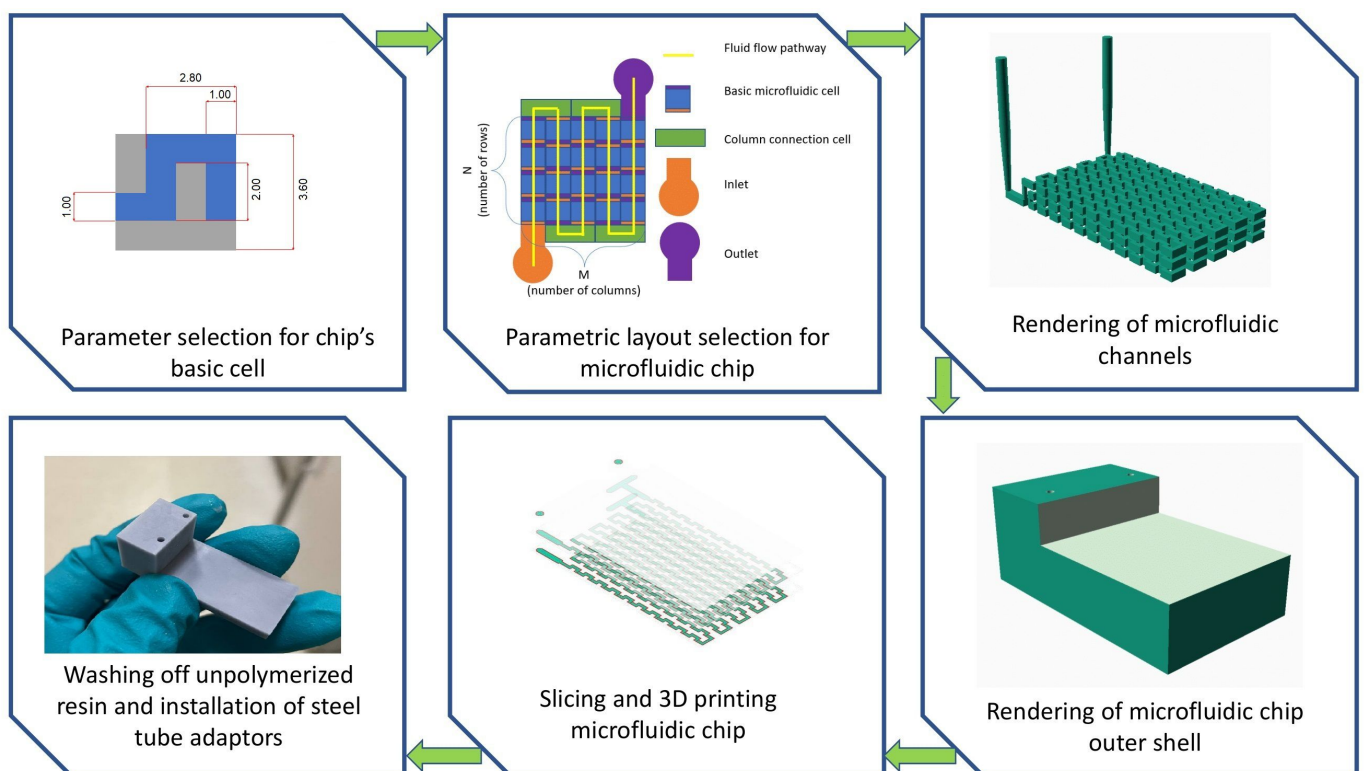


Figure 1. Schematic of formation of three-dimensional microfluidic chips.

One of the requirements for the microfluidic chip to be created is the ability to reproduce a large number of syntheses. Attempts to reduce the cross-sectional size caused destruction of the channels. Therefore, a cross-section of 1 mm^2 was chosen in order to avoid channel plugging and increase the chip's lifetime. The length of internal channels and volume of the chip are 1080 mm and 1.8 mL, respectively. In this work, it is planned to change the thermal treatment time by changing the rate of precursor injection into the microfluidic chip. The time for classical QD AIS synthesis in the flask is approximately 30 min (1800 s). Since the microfluidic chip should be compact, internal channels with a total volume of 1.8 mL were created. It allows 1 mL of precursors to flow through an internal volume in 30 min. To ensure the compactness of the chip, the base cells composing the channel were arranged in a three-dimensional matrix of $(6 \times 10 \times 5)$ elements. An inlet channel and an outlet channel were connected to the main channel for fluid input and to the outlet channels of the microfluidic chip.

Figure 1 shows a 3D model of the microfluidic chip in a section and photos of chips formed using photopolymer 3D printing. To form physical copies of the chips using additive manufacturing techniques, the chip design was subtracted from the solid block, thus forming the cavities of the microfluidic channels. Microfluidic chips were printed on a 3D printer using Phrozen TR250LV photopolymer resin (Phrozen, Taiwan, China). The choice of this photopolymer resin is justified by its outstanding physical and mechanical characteristics compared with the usual photopolymer resins used in 3D printing. In particular, after photopolymerization, this resin is characterized by an increased mechanical tensile strength in the temperature range from 0 to $100\text{ }^\circ\text{C}$, which is ideal for use in hydrothermal types of nanoparticles synthesis, where the temperature inside the reactor reaches $90\text{ }^\circ\text{C}$.

The chip printing parameters for this photopolymer resin were as follows: the thickness of one layer and irradiation time per layer were $50\text{ }\mu\text{m}$ and 2 s, respectively. After printing finalization, the channels of the chip and its surface contained a large amount of unpolymerized resin. To remove it, the chip was placed in a bath filled with isopropanol and exposed to ultrasound for 10 min. After that, the internal channels of the chip were flushed with pure isopropanol using a syringe pump connected to the chip inlet.

The syringe pumps were connected to the microfluidic chip using Teflon tubes with inner and outer diameters of 1 and 1.5 mm, and steel adapters with inner and outer diameters of 0.9 and 1.1 mm, respectively. The microfluidic chip connection itself was performed in two stages. At the first stage, the steel adapter was inserted into the Teflon tube with one end, and the other end was inserted into the inlet or outlet port of the microfluidic chip. At the second stage, to seal the chip, all joints were smeared with several layers of photopolymer resin followed by polymerization of the joints using UV light irradiation with a wavelength of 405 nm for 10–30 s.

3.2. Synthesis of AIS Quantum Dots in a Microfluidic Chip

The amount of precursors and their ratio was the same for microfluidic and classical syntheses (Section 2). In the case of classical hydrothermal synthesis, the precursor mixture was placed in a three-head flask, which was further subjected to stirring and thermal treatment. In the second case, to heat the reagents, the microfluidic chip was placed in a water bath mounted on a heating element. The temperature of water in the flask and in the chip was set to 40, 60, and $90\text{ }^\circ\text{C}$ and was maintained by feedback from the heating element and the temperature sensor located in the water bath. These temperature regimes were chosen to compare the optical properties of AIS QD. According to the synthetic protocol [17], the duration of thermal treatment synthesis is about 30 min. Therefore, a 1800 s treatment time was used as a starting point for both classical and microfluidic synthesis for an explicit comparison in efficiencies between these two types of synthesis. Additionally, 180 and 18 s treatment times were used to establish the dependence of the optical properties of quantum dots on the precursor treatment time. In order to sustain such treatment time in microfluidic devices, various precursor feeding rates were used,

thereby precisely adjusting the temperature exposure time of the precursor solution. The precursor mixture was fed using a syringe pump at 0.001, 0.01 and 0.1 mL/s. It allows the same volume of precursor mixture, i.e., 1 mL, to pass through our chip in 18, 180, and 1800 s, respectively. After synthesis, QDs solutions were washed with the addition of isopropyl alcohol in a 1:2 ratio and centrifuged for 3 min at $12,000 \text{ min}^{-1}$. Then, they were redissolved in water. It is noteworthy that all syntheses were carried out in one chip. After the eight syntheses mentioned in this work, no external macromechanical damage was found. All connections of Teflon hoses that supply and divert precursor solution to the microfluidic reactor remained sealed. This confirms the possibility of extended utilization of such reactors in syntheses carried out at the temperature of up to 90°C .

3.3. Dependence of AgInS_2 QD Optical Properties on Synthesis Temperature

Figure 2 shows the absorption and photoluminescence (PL) spectra of the AIS QDs synthesized in the microfluidic chip at 40°C , 60°C , and 90°C for 1800 s.

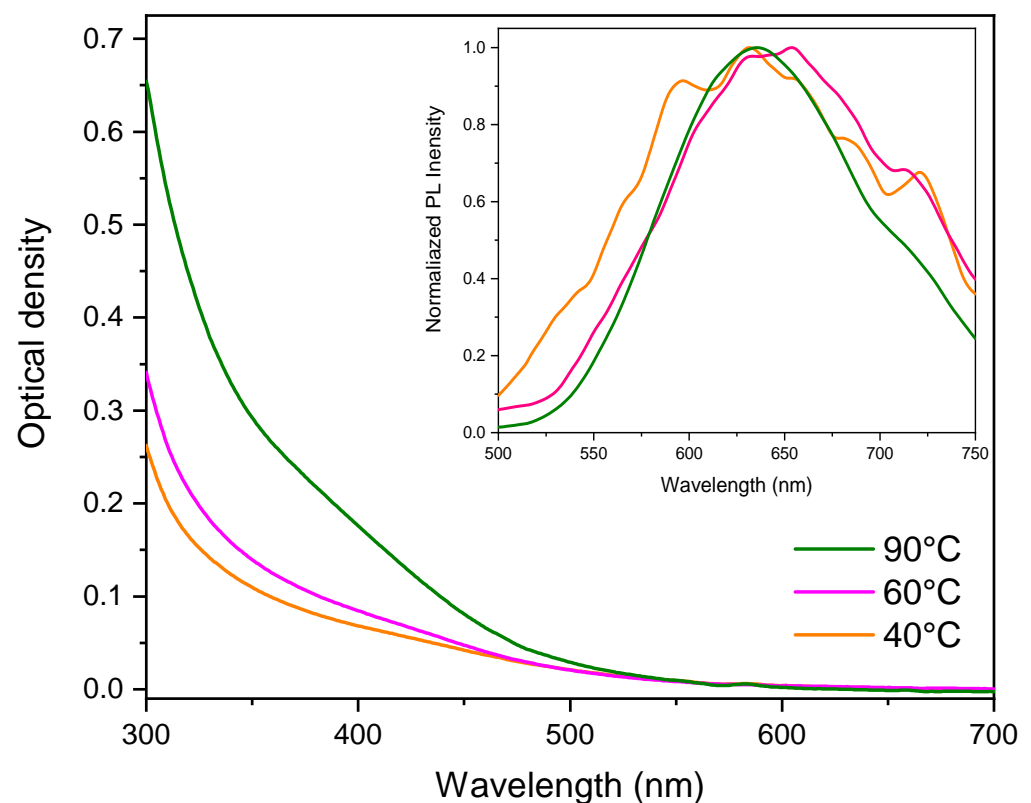


Figure 2. Absorption and normalized PL spectra (the inset) of AgInS_2 quantum dots synthesized in a microfluidic chip; PL excitation wavelength is 405 nm.

Figure 2 shows that the microfluidic synthesized ensembles of AIS quantum dots demonstrate typical absorption and PL spectra for ternary QDs [19,20]. It is well postulated that the complex shape of the PL band of AIS QDs is attributed to several radiative transitions [17]. Luminescence in AgInS_2 and CuInS_2 QDs is primarily attributed to defects in the crystal lattice of sulfur, indium, silver, and copper atoms, rather than excitonic processes [21]. The presence of a long-wave luminescence shoulder is a result of the recombination of the electron–hole pair at defective indium sites [22].

It is not surprising that increasing the temperature of QD synthesis leads to increased optical density in the QD absorption spectrum because of increase in precursor reaction rates [23] and improvement in QD crystallinity [24]. PLQY of QD ensembles estimated in a comparative method with Rhodamine 6G as the reference demonstrates the linear dependence on synthesis time, as shown in Figure 3.

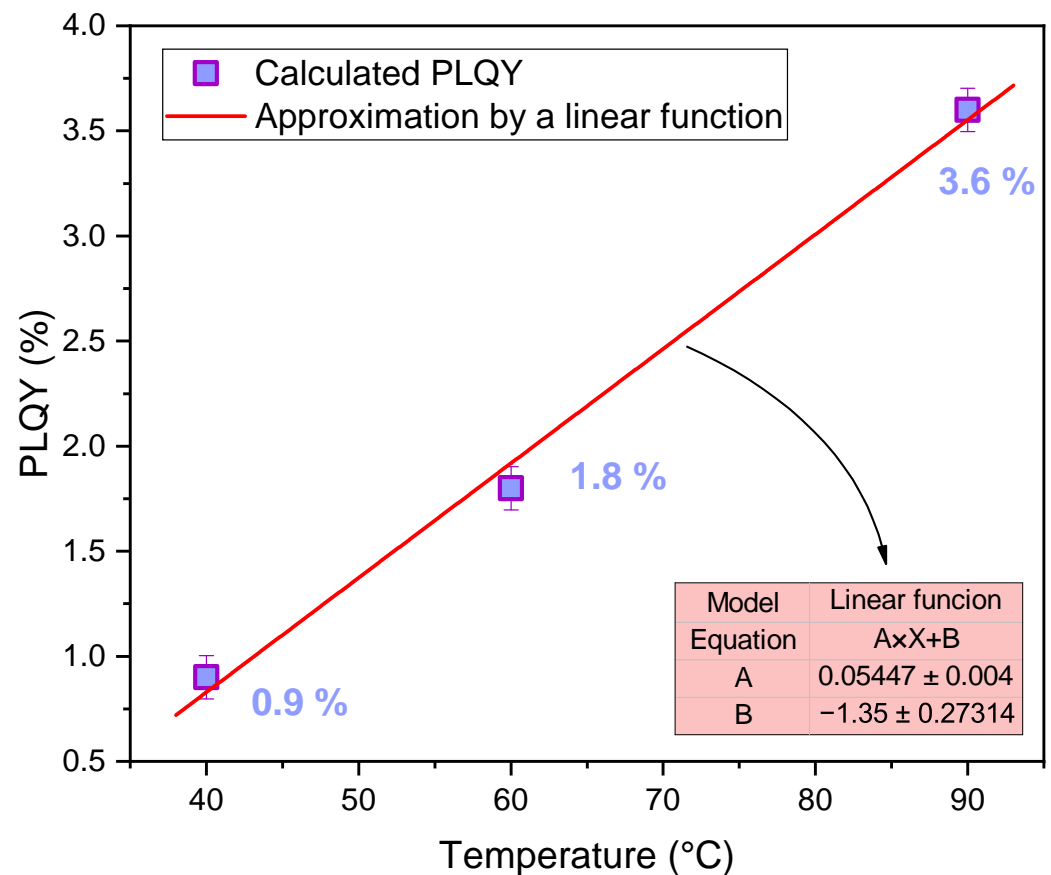


Figure 3. The dependence of the PLQY of the AIS QDs synthesized for 1800 s on the synthesis temperature and its linear fitting.

Figure 3 shows that increase in the synthesis temperature of AgInS₂ QDs leads to a linear increase in PLQY. The PL quantum yield of samples synthesized in the microfluidic chip at 40, 60, and 90 °C was 0.9, 1.8, and 3.6%, respectively. Since the microfluidic synthesis of the AIS QDs at 90 °C allows achieving the best PLQY in the range of 40–90 °C, this temperature was used for 18 and 180 s QDs synthesis and for the study on how synthesis time impacts QD optical properties and their yield.

3.4. Impact of Synthesis Time on the Optical Properties of AgInS₂ QDs

Figure 4 presents the absorption and photoluminescence excitation (PLE) spectra of AgInS₂ QD synthesized in a microfluidic chip and in a flask at 90 °C for precursor thermal treatment times of 18, 180, and 1800 s in the reactor.

AIS QDs synthesized in our microfluidic chip demonstrate a more pronounced optical absorption edge band in comparison with QDs synthesized in a flask (Figure 4a,b). Typically, electronic absorption bands of QDs are more sharp in their PLE spectra [25]. It allows using PLE spectra (Figure 4c,d) of QDs to estimate the absorption edge band position of QDs more correctly in comparison with their absorption spectra. Our data clearly show that increasing the synthesis time of up to 1800 s in the microfluidic chip leads to the shift in the QD absorption band to higher energy because of decreasing QD size [26].

Figure 5 presents normalized PL spectra of AgInS₂ quantum dots synthesized in a microfluidic chip and in a flask at 90 °C for precursor thermal treatment times of 18, 180, and 1800 s in the reactor.

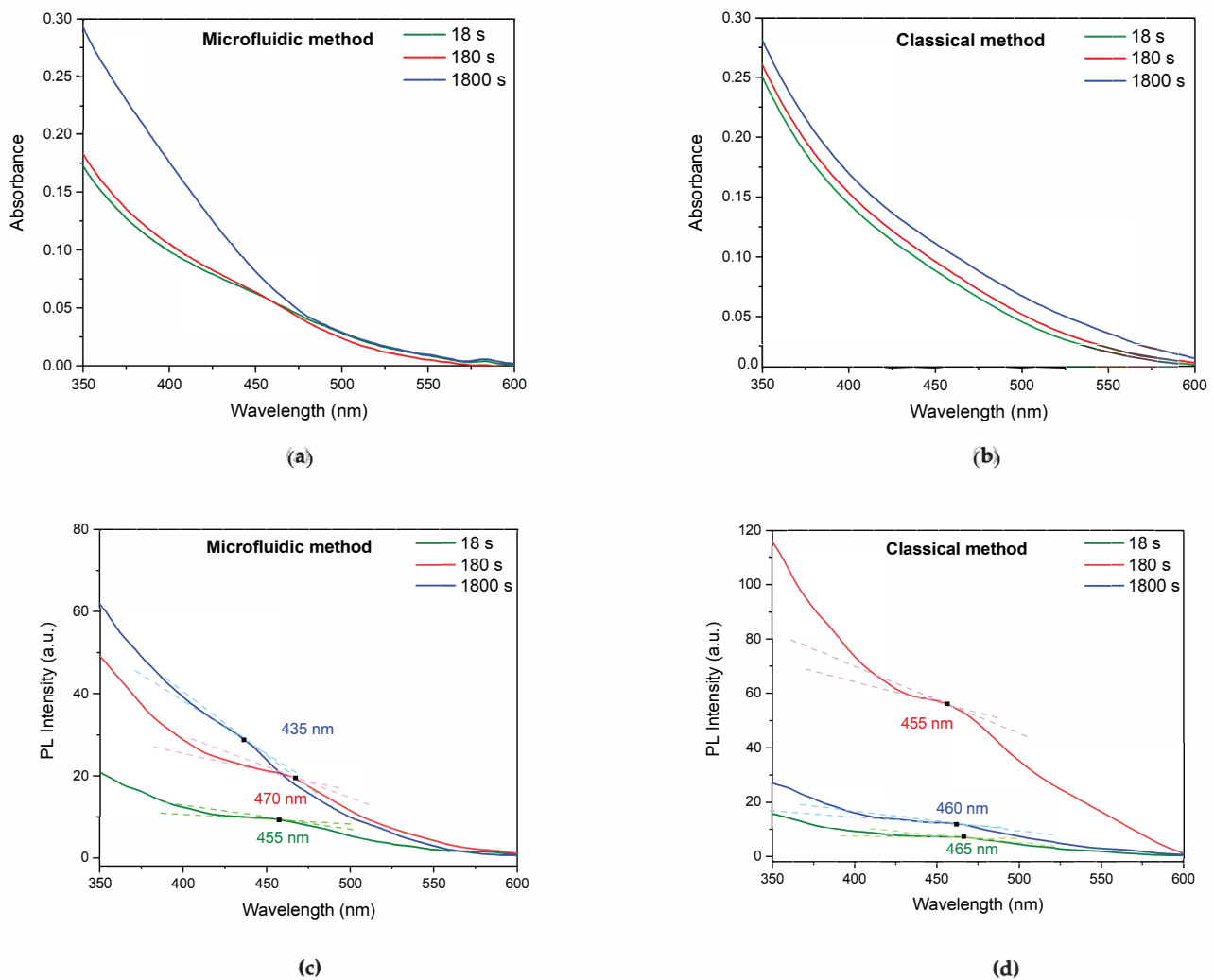


Figure 4. Absorption (a,b) and PLE (c,d), spectra of the AIS QDs synthesized in a microfluidic chip and by classical hydrothermal method in a flask at 90 °C and different thermal treatment times. PL acquisition wavelength is 610 nm.

Figure 5 shows that QDs synthesized in a flask exhibit classical dynamics of nanocrystal growth accompanied by a gradual increase in luminescence intensity and a long-wave shift of the PL band [27]. The PL band shift to the higher energy region because of increasing microfluidic synthesis time correlates very well with the shift of PL band absorption spectrum (Figure 4) and suggests the decrease in QD size.

Thermal treatment times of 18, 180, and 1800 s correspond to precursor injection rates of 0.1, 0.01, and 0.001 mL, respectively. Such rates ensure the laminar fluid flow [28]; therefore, the reagents in the channel mix mainly by diffusion and convection of molecules under the influence of ambient temperature. According to [19,26,29], the shift of the QD PL band to the higher-energy region indicates a decrease in the proportion of silver atoms in the AIS QDs and disappearance of the shoulder in the PL band of AIS QDs located at 700 nm.

A comprehensive study of the optical and photophysical properties of the AIS quantum dots in [26] allows us to suggest that the average size of our QDs is varied from 1.4 to 2 nm because of the QD absorption (Figure 4) and PL spectra (Figure 5).

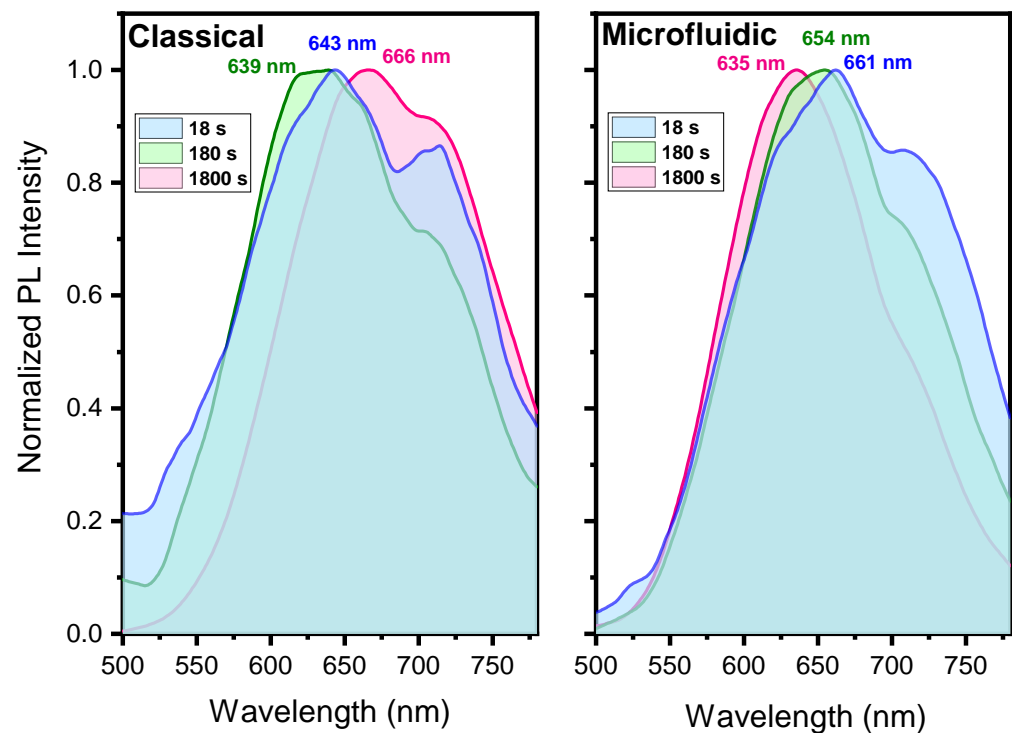


Figure 5. Normalized PL spectra of the AIS QDs synthesized in a microfluidic chip and by classical hydrothermal method in a flask at 90 °C and different thermal treatment times, PL excitation wavelength is 405 nm.

Figure 6 shows the dependence of the PL QY of the classical and microfluidic syntheses of AIS QDs on the synthesis time.

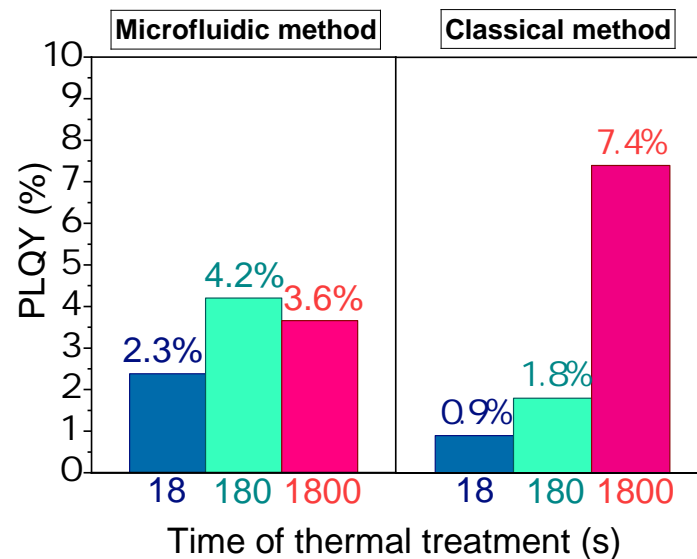


Figure 6. Dependence of PLQY of AIS QDs synthesized at 90 °C on the synthesis time in the microfluidic chip and in a flask.

It was found that PLQY of AIS QDs synthesized with the classical approach reaches 7.4%. It correlates very well with the PLQY of typical hydrophilic AIS QDs [30]. The best QY PL for our AIS QDs synthesized in the microfluidic chip is close to 4%. The increase in microfluidic synthesis time up to 1800 s not only reduces the QD size, shifts absorption and PL bands to higher energy, and decreases PL bandwidth, but also slightly decreases their

PLQY. Our data demonstrate that PLQY of QDs synthesized in the microfluidic chip for 18 and 180 s is 2.5 times higher than for QDs synthesized in a flask for the same time (Figure 6). It is assumed that the difference in dependencies of PLQY of QDs on synthesis time for microfluidic and classical syntheses is related to the high coefficient of mass temperature transfer in the reagent mixture in the microfluidic chip [31].

Figure 7 shows the dependences of the AIS QD PL kinetics of QD synthesized by hydrothermal and microfluidic methods on the synthesis time. The experimental data were approximated with three-exponential functions according to Formula (2).

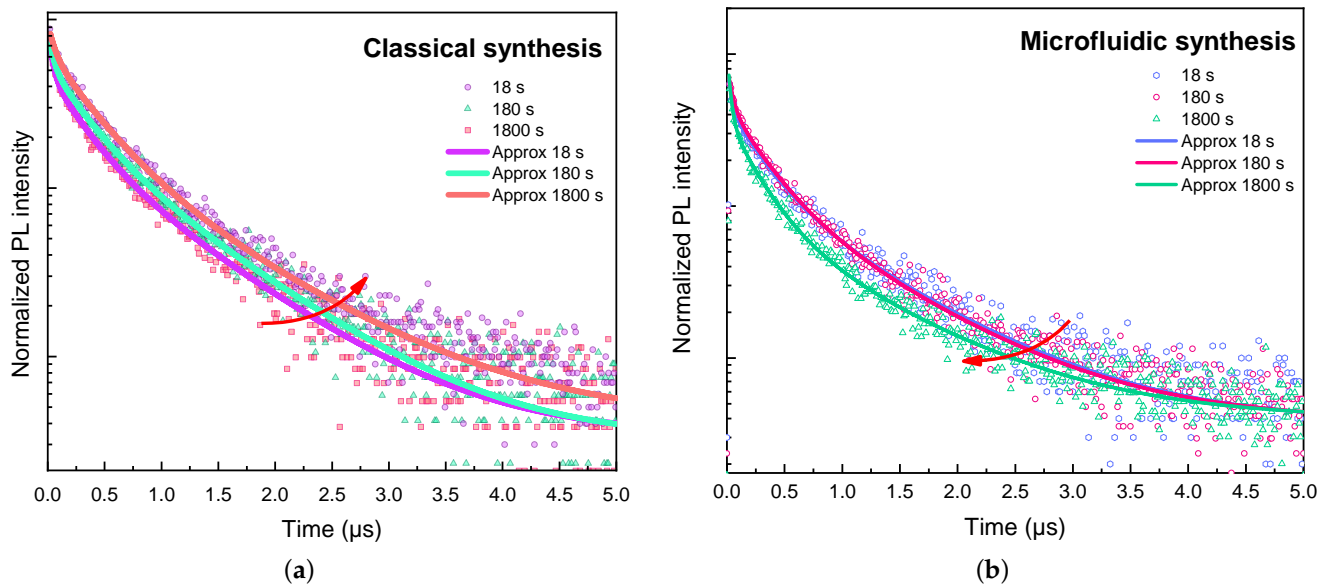


Figure 7. PL decay curves of AIS QDs synthesized at 90 °C during 18 s, 180 s, and 1800 s: (a) classical and (b) microfluidic syntheses. Red arrows show the dynamics of decay curves with changes in heat treatment time.

PL decay curves for all AIS QD samples shown in Figure 7 were fitted with three-exponential functions which is typical for ternary QDs [32]. The fitting parameters of PL decay curves for all AIS QD samples are presented in Table 1.

Table 1. The fitting parameters of PL decay curves for AIS QD samples.

Type of Synthesis	Time of Synthesis, s	τ_1 , ns	τ_2 , ns	τ_3 , ns	A_1 , %	A_2 , %	A_3 , %
Classical	18	35 ± 3	273 ± 13	818 ± 21	39.3	41.5	39.2
Classical	180	42 ± 3	219 ± 9	810 ± 13	31.5	46.1	22.4
Classical	1800	55 ± 5	370 ± 11	1026 ± 35	24.3	52.6	23.1
Microfluidic	18	32 ± 2	276 ± 10	911 ± 25	36.4	43.9	19.8
Microfluidic	180	40 ± 3	287 ± 6	915 ± 12	35.3	45.6	19.1
Microfluidic	1800	28 ± 1	249 ± 5	993 ± 15	46.2	38.6	15.3

The analysis of PL decay curves of classical synthesized AIS QDs shows that an increase in the synthesis time from 18 to 1800 s leads to an increase in all characteristic PL decay times. This trend correlates very well with the increase in PLQY because of increasing synthesis time (see Figure 6). The correlation of characteristic PL decay times with PLQY also remains for microfluidic-synthesized AIS QDs for the shortest (30–40 ns) and the middle (250–290 ns) components, but not for the longest component (900–1000 ns). The increase in characteristic PL decay times can indicate an improved surface quality or an increase in size of the synthesized QDs [33]. The shortest PL decay time belongs to

defects of the crystal lattice [34]. Therefore, it can be an effective marker of the quality of the QD surface. The data presented in Table 1 clearly indicate a gradual decrease in the number of defects on the surface of QDs synthesized by the microfluidic method due to a decrease in the contribution of the short-lived component of QDs luminescence. It is worth noting that, according to the already published works, the long-lived components of the three-component QDs luminescence (about 100–900 ns) belong to the luminescence at the donor–acceptor pair transitions [22].

The ratio of yield of QDs synthesized at different regimes in a microfluidic chip and a flask can be estimated because the same volume of precursor mixtures with the same precursor concentrations was used in all our syntheses (for details, see Appendix A). QDs are nanocrystals whose absorption spectra depend on QD size because of the quantum confinement effect [35]. This fact is widely used to estimate the Cd-based QD size and extinction coefficients [36]. Although absorption spectra of ternary QDs based on silver or copper contain no sharp bands, this approach has also been applied to estimate their sizes and extinction coefficients. It was demonstrated that the position of the fundamental edge in CIS QD absorption spectra allows estimating QD size and extinction coefficient [18]. It is well known that stoichiometry, electronic structure and optical properties of CIS and AIS QDs are very similar [37]. Therefore, the concentration of our QD samples was estimated using the absorption, PL and PLE spectra of our spectra. For details of QD concentration estimation of our samples, refer to Appendix A. Table 2 accumulates the absorption band position (ABP), molar extinction coefficient (MEC), and QD concentration.

Table 2. Calculations of the concentration of AIS QD solutions prepared by microfluidic synthesis and by classical hydrothermal synthesis at 90 °C with treatment times of 18, 180 and 1800 s.

Type of Synthesis	Time of Synthesis, s	ABP, nm	MEC, $10^5 \text{ M}^{-1} \text{ cm}^{-1}$	Optical Density	Concentration, 10^{-6} M
Classical	18	465	0.12692	0.063	4.9
Classical	180	455	0.10944	0.088	8.6
Classical	1800	460	0.13753	0.097	7.1
Microfluidic	18	455	0.10944	0.057	5.2
Microfluidic	180	470	0.13217	0.049	3.7
Microfluidic	1800	435	0.09269	0.105	11.3

According to the data presented in Table 2 and Appendix A, the relative QD yield ratio of classical and microfluidic synthesis strongly depends on their synthesis time. The relative yield of the AIS quantum dot product is about 1.6, 0.4, 1 for heat treatment times of 1800, 180, and 18 s, respectively. It is intriguing that the QD yields in classical and microfluidic syntheses are the same for the shortest synthesis time, i.e., 18 s. It means that the efficiency of precursor mixing is about the same for both classical and microfluidic syntheses and there are no advantages to using the latter one. In contrast, our data demonstrate that increasing the synthesis time up to 180 s leads to a strong decrease of the QD yield ratio. Therefore, despite the relatively good PLQY of AIS QDs synthesized with microfluidic approach, it is suggested that 180 s is not optimal for microfluidic synthesis of AIS QDs in our chip. At the same time, our data strongly confirm the increase in QD synthesis yield up to 60% in comparison with classical one if typical classical AIS QD synthesis time [17] is used.

4. Conclusions

This study introduces a novel technique for the flow hydrothermal synthesis of three-component AgInS_2 quantum dots using additive manufacturing to form microfluidic chips. It demonstrates the capability of operating photopolymer resin-based chips for prolonged durations without developing any structural defects that could compromise the mechanical properties of the microfluidic chip channels. Based on our analysis of the photophysical properties of the AIS QDs, the microfluidic chip exhibited a significantly

higher coefficient of mass and heat transfer compared to the conventional flask reactor. The photoluminescence quantum yield of samples synthesized by the microfluidic method for 18 and 180 s is found to be about 2.5 times higher than that for QDs synthesized in a flask for the same time. It is demonstrated that the product yield of AIS quantum dots synthesized in the microfluidic chip is up to 60% higher than in a flask for the treatment time, which is typical for AIS QD classical synthesis, i.e., 1800 s.

Author Contributions: Conceptualization, I.R., K.B. and A.O.; methodology, I.R.; writing—original draft preparation and investigation, K.B., I.R. and S.K.; formal analysis, J.W.S. and S.M.; validation and supervision, A.O. All authors have read and agreed to the published version of the manuscript.

Funding: This work was financially supported by Ministry of Education and Science of the Russian Federation: State assignment, Passport 2019-1080 (Goszadanie 2019-1080) , and by RPMA grant of School of Physics and Engineering of ITMO University (N° 621317).

Institutional Review Board Statement: Not applicable.

Informed Consent Statement: Not applicable.

Data Availability Statement: Data is available upon request.

Conflicts of Interest: The authors declare no conflict of interest.

Appendix A

Since the optical properties and structure of the AIS and CIS QDs are similar, and the number of works aimed at studying the optical properties of the CIS QDs prevails, the observed optical properties can be explained in the first approximation by generalizing the existing results about the CIS QDs to the AIS QDs. To determine the concentration of the solutions, this approximation was used. In work [18], the dependence of the CIS QD size on the wavelength of the fundamental absorbance edge (WFAE) and the dependence of the CIS QD size on the molar extinction coefficient (MEC) were experimentally obtained. Thus, the known location of the absorption band position of AIS QD allows us to determine the concentration of nanoparticles, given their size, via the Bouguer–Lambert–Beer Formula (A1):

$$D = C \cdot \varepsilon \cdot l, \quad (\text{A1})$$

where D is optical density; ε is a molar extinction coefficient; l is distance; C is concentration.

In order to determine the WFAE, two tangents to the graph of the luminescence excitation intensity spectra were plotted (Figure 4c,d). The obtained wavelengths were compared with the particle size [18] and are written in Table 2. The resulting AIS QD sizes were compared with the extinction coefficients in work [18] used to determine the concentration. Then, using the absorption spectra (Figure 4a,b), the optical densities were determined. Using Formula (A1), concentrations were obtained, provided that l is 1 cm.

To determine the relative yield of the AIS quantum dot product, the ratio of concentrations of samples obtained by different methods for the same heat treatment time was calculated. Thus, the microfluidic synthesis/classical synthesis ratio is about 1.6, 0.4, 1 for heat treatment times of 1800, 180, and 18 s, respectively.

References

1. Mi, W.; Tian, J.; Tian, W.; Dai, J.; Wang, X.; Liu, X. Temperature dependent synthesis and optical properties of CdSe quantum dots. *Ceram. Int.* **2012**, *38*, 5575–5583. [[CrossRef](#)]
2. Bian, F.; Sun, L.; Cai, L.; Wang, Y.; Zhao, Y. Quantum dots from microfluidics for nanomedical application. *Wiley Interdiscip. Rev. Nanomed. Nanobiotechnol.* **2012**, *11*, 1567. [[CrossRef](#)]
3. Abedini-Nassab, R.; Pouryosef Miandoab, M.; Şaşmaz, M. Microfluidic Synthesis, Control, and Sensing of Magnetic Nanoparticles: A Review. *Micromachines* **2021**, *12*, 768. [[CrossRef](#)]
4. Shepherd, S.J.; Issadore, D.; Mitchell, M.J. Microfluidic formulation of nanoparticles for biomedical applications. *Biomaterials* **2021**, *274*, 120826. [[CrossRef](#)]
5. Niculescu, A.-G.; Chircov, C.; Bircă, A.C.; Grumezescu, A.M. Nanomaterials Synthesis through Microfluidic Methods: An Updated Overview. *Nanomaterials* **2021**, *11*, 864. [[CrossRef](#)] [[PubMed](#)]

6. Ma, J.; Lee, S.M.-Y.; Yi, C.; Li, C.-W. Controllable synthesis of functional nanoparticles by microfluidic platforms for biomedical applications—A review. *Lab Chip* **2017**, *17*, 209–226. [[CrossRef](#)]
7. Lai, X.; Lu, B.; Zhang, P.; Zhang, X.; Pu, Z.; Yu, H.; Li, D. Sticker Microfluidics: A Method for Fabrication of Customized Monolithic Microfluidics. *Acs Biomater. Sci. Eng.* **2019**, *5*, 6801–6810. [[CrossRef](#)] [[PubMed](#)]
8. Kajtez, J.; Buchmann, S.; Vasudevan, S.; Birtele, M.; Rocchetti, S.; Pless, C.J.; Heiskanen, A.; Barker R.A.; Martínez-Serrano, A.; Parmar, M.; et al. 3D-Printed Soft Lithography for Complex Compartmentalized Microfluidic Neural Devices. *Adv. Sci.* **2020**, *7*, 2198–3844. [[CrossRef](#)] [[PubMed](#)]
9. Ma, H.; Pan, L.; Wang, J.; Zhang, L.; Zhang, Z. Synthesis of AgInS₂ QDs in droplet microreactors: Online fluorescence regulating through temperature control. *Chin. Chem. Lett.* **2019**, *30*, 79–82. [[CrossRef](#)]
10. Weisgrab, G.; Ovsianikov, A.; Costa, P.F. Functional 3D Printing for Microfluidic Chips. *Adv. Mater. Technol.* **2019**, *4*, 1900275. [[CrossRef](#)]
11. Cheng, Y.; Ling, S.D.; Geng, Y.; Wang, Y.; Xu, J. Microfluidic synthesis of quantum dots and their applications in bio-sensing and bio-imaging. *Nanoscale Adv.* **2021**, *3*, 2180–2195. [[CrossRef](#)] [[PubMed](#)]
12. Girma, W.M.; Fahmi, M.Z.; Permadi, A.; Abate, M.A.; Chang, J.-Y. Synthetic strategies and biomedical applications of I–III–VI ternary quantum dots. *J. Mater. Chem.* **2021**, *5*, 6193–6216. [[CrossRef](#)]
13. May, B.M.; Bambo, M.F.; Hosseini, S.S.; Sidwaba, U.; Nxumalo, E.N.; Mishra, A.K. A review on I–III–VI ternary quantum dots for fluorescence detection of heavy metals ions in water: Optical properties, synthesis and application. *RSC Adv.* **2022**, *12*, 11216–11232. [[CrossRef](#)] [[PubMed](#)]
14. Baranov, K.; Kolesova, E.; Baranov, M.; Orlova, A. Generation of Reactive Oxygen Species by AgInS₂/TiO₂ Nanocomposites upon Exposure to UV and Visible Radiation. *Opt. Spectrosc.* **2022**, *130*, 1562–6911. [[CrossRef](#)]
15. Wang, G.; Jin, W.; Qasim, A.M.; Gao, A.; Peng, X.; Li, W.; Feng, H.; Chu, P.K. Antibacterial effects of titanium embedded with silver nanoparticles based on electron-transfer-induced reactive oxygen species. *Biomaterials* **2017**, *124*, 25–34. [[CrossRef](#)]
16. Mir, I.A.; Radhakrishnan, V.S.; Rawat, K.; Prasad, T.; Bohidar, H.B. Bandgap Tunable AgInS based Quantum Dots for High Contrast Cell Imaging with Enhanced Photodynamic and Antifungal Applications. *Sci. Rep.* **2018**, *8*, 9322. [[CrossRef](#)]
17. Raevskaya, A.; Lesnyak, V.; Haubold, D.; Dzhagan, V.; Stroyuk, O.; Gaponik, N.; Zahn, D.R.T.; Eychmüller, A. A Fine Size Selection of Brightly Luminescent Water-Soluble Ag-In-S and Ag-In-S/ZnS Quantum Dots. *J. Phys. Chem.* **2017**, *121*, 9032–9042. [[CrossRef](#)]
18. Qin, L.; Li, D.; Zhang, Z.; Wang, K.; Ding, H.; Xie, R.; Yang, W. The determination of extinction coefficient of CuInS₂, and ZnCuInS₃ multinary nanocrystals. *Nanoscale* **2012**, *4*, 6360. [[CrossRef](#)]
19. Hu, X.; Chen, T.; Xu, Y.; Wang, M.; Jiang, W.; Jiang, W. Hydrothermal synthesis of bright and stable AgInS₂ quantum dots with tunable visible emission. *J. Lumin.* **2018**, *200*, 189–195. [[CrossRef](#)]
20. May, B.M.M.; Parani, S.; Oluwafemi, O.S. Detection of Ascorbic Acid using Green Synthesized AgInS₂ Quantum Dots. *Mater. Lett.* **2018**, *236*, 432–435. [[CrossRef](#)]
21. Zang, H.; Li, H.; Makarov, N.S.; Velizhanin, K.A.; Wu, K.; Park, Y.-S.; Klimov, V.I. Thick-Shell CuInS₂/ZnS Quantum Dots with Suppressed “Blinking” and Narrow Single-Particle Emission Line Widths. *Nano Lett.* **2017**, *17*, 1787–1795. [[CrossRef](#)]
22. Fu, M.; Luan, W.; Tu, S.-T.; Mleczko, L. Optimization of the recipe for the synthesis of CuInS₂/ZnS nanocrystals supported by mechanistic considerations. *Green Process. Synth.* **2017**, *6*, 133–146. [[CrossRef](#)]
23. Zikalala, N.; Parani, S.; Tsolekile, N.; Oluwafemi, O.S. Facile green synthesis of ZnInS quantum dots: Temporal evolution of their optical properties and cell viability against normal and cancerous cells. *J. Mater. Chem.* **2020**, *8*, 9329–9336. [[CrossRef](#)]
24. Mahmoud, W.E.; Yagmour, S.J. The temporal evolution of the structure and luminescence properties of CdSe semiconductor quantum dots grown at low temperatures. *J. Lumin.* **2012**, *132*, 2447–2451. [[CrossRef](#)]
25. Tonti, D.; van Mourik, F.; Chergui, M. On the Excitation Wavelength Dependence of the Luminescence Yield of Colloidal CdSe Quantum Dots. *Nano Lett.* **2014**, *4*, 2483–2487. [[CrossRef](#)]
26. Stroyuk, O.; Raievska, O.; Kupfer, C.; Solonenko, D.; Osvet, A.; Batentschuk, M.; Brabec, C.J.; Zahn, D.R.T. High-Throughput Time-Resolved Photoluminescence Study of Composition- and Size-Selected Aqueous Ag-In-S Quantum Dots. *J. Phys. Chem.* **2021**, *125*, 12185–12197. [[CrossRef](#)]
27. Cheng, O.H.-C.; Qiao, T.; Sheldon, M.T.; Son, D.H. Size- and Temperature-dependent Photoluminescence Spectra of Strongly Confined CsPbBr₃ Quantum Dots. *Nanoscale* **2020**, *12*, 13113–13118. [[CrossRef](#)]
28. Song, Y.; Hormes, J.; Kumar, C.S.S.R. Size- and Temperature-dependent Microfluidic Synthesis of Nanomaterials. *Small* **2008**, *4*, 698–711. [[CrossRef](#)]
29. Moodelly, D.; Kowalik, P.; Bujak, P.; Pron, A.; Reiss, P. Synthesis, photophysical properties and surface chemistry of chalcopyrite-type semiconductor nanocrystals. *J. Mater. Chem.* **2019**, *7*, 11665–11709. [[CrossRef](#)]
30. Kang, X.; Huang, L.; Yang, Y.; Pan, D. Scaling up the Aqueous Synthesis of Visible Light Emitting Multinary AgInS₂/ZnS Core/Shell Quantum Dots. *J. Phys. Chem.* **2015**, *119*, 7933–7940. [[CrossRef](#)]
31. Wang, J.; Shao, C.; Wang, Y.; Sun, L.; Zhao, Y. Microfluidics for Medical Additive Manufacturing. *Engineering* **2020**, *6*, 1244–1257. [[CrossRef](#)]
32. Lazareva, A.A.; Reznik, I.A.; Dubavik, A.Y.; Veniaminov A.V.; Orlova A.O. Investigation of photoluminescence kinetics CuInS₂/ZnS quantum dots. *J. Phys. Conf. Ser.* **2021**, *2058*, 012007. [[CrossRef](#)]

33. Sun, J.; Ikezawa, M.; Wang, X.; Jing, P.; Li, H.; Zhao, J.; Masumoto, Y. Photocarrier recombination dynamics in ternary chalcogenide CuInS₂ quantum dots. *Phys. Chem. Chem. Phys.* **2015**, *17*, 11981–11989. [[CrossRef](#)]
34. Motevich, I.G.; Zenkevich, E.I.; Stroyuk, A.L.; Raevskaya, A.E.; Kulikova, O.M.; Sheinin, V.B.; Koifman, O.I.; Zahn, D.R.T.; Strekal, N.D. Effect of pH and Polyelectrolytes on the Spectral-Kinetic Properties of AIS/ZnS Semiconductor Quantum Dots in Aqueous Solutions. *J. Appl. Spectrosc.* **2021**, *87*, 1057–1066. [[CrossRef](#)]
35. Empedocles, S.A.; Norris, D.J.; Bawendi, M.G. Photoluminescence Spectroscopy of Single CdSe Nanocrystallite Quantum Dots. *Phys. Rev. Lett.* **1996**, *77*, 3873–3876. [[CrossRef](#)]
36. Yu, W.W.; Qu, L.; Guo, W.; Peng, X. Experimental Determination of the Extinction Coefficient of CdTe, CdSe, and CdS Nanocrystals. *Chem. Mater.* **2003**, *15*, 2854–2860. [[CrossRef](#)]
37. Liu, L.; Hu, R.; Law, W.-C.; Roy, I.; Zhu, J.; Ye, L.; Hu, S.; Zhang, X.; Yong, K.-T. Optimizing the synthesis of red- and near-infrared CuInS₂ and AgInS₂ semiconductor nanocrystals for bioimaging. *Analyst* **2013**, *138*, 6140. [[CrossRef](#)]

Disclaimer/Publisher’s Note: The statements, opinions and data contained in all publications are solely those of the individual author(s) and contributor(s) and not of MDPI and/or the editor(s). MDPI and/or the editor(s) disclaim responsibility for any injury to people or property resulting from any ideas, methods, instructions or products referred to in the content.